The Turbulence Structure in a Continental Stratocumulus Cloud from Millimeter-Wavelength Radar Observations

PAVLOS KOLLIAS AND BRUCE ALBRECHT

Rosenstiel School of Marine and Atmospheric Sciences, University of Miami, Miami, Florida

(Manuscript received 16 March 1999, in final form 22 September 1999)

ABSTRACT

The turbulent-scale vertical velocity structure in a continental stratocumulus cloud is studied using a 3-mm wavelength Doppler radar operating in a vertically pointing mode. The radar observations provided 30-m sampling in the vertical with 2-s averages of 10 000 samples. Vertical velocity measurements were made continuously for an 8-h period and were further supported by measurements of cloud-base height from a laser ceilometer and liquid water path from a microwave radiometer. During the beginning of the observational period, the cloud layer extended between 200 and 800 m. The vertical velocity variance profiles evolved systematically over the period from a well-defined peak in the upper part of the cloud layer of $\sim$0.7 $m^2 s^{-2}$ to a peak in the lower part of the cloud layer of 0.2 $m^2 s^{-2}$ as the layer became decoupled later in the observing period. The vertical velocity skewness during the well-coupled conditions was negative through most of the cloud, consistent with the presence of relatively narrow downdrafts. A positive skewness in the top 100 m of the cloud is consistent with relatively narrow penetrating updrafts at this level.

The radar vertical velocities are used to compare the directly observed updraft fractional coverage and mass flux with those obtained from the bulk statistics. These comparisons are consistent with similar comparisons made using a large eddy simulation model. The fractional coverage and the mass flux associated with coherent updraft structures are obtained for a range of criteria used to define the updrafts. A more detailed analysis of the vertical velocities in the cloud confirms the existence of well-defined downdrafts extending through the entire cloud depth. These downdrafts are estimated to have horizontal dimensions of about 200 m and appear to originate on the downshear side of updrafts. The reduction of radar reflectivity at cloud top in the downdrafts is consistent with the entrainment of drier air. This study further illustrates the utility of millimeter-wavelength radars for studying turbulence in boundary layer clouds and particularly in defining the vertical structure of coherent eddies.

1. Introduction

Stratocumulus clouds play an important role in the climate system. They are efficient reflectors of shortwave radiation and cover extensive areas of the earth's surface. As a result, these clouds contribute substantially to the global estimate of cloud radiative forcing (Ramanathan et al. 1989). A number of studies have focused on marine stratocumulus clouds during the past 20 yr. These efforts have increased our observational basis for understanding the processes operating in these clouds (e.g., Albrecht et al. 1985) and have stimulated a variety of modeling studies to better understand the nature of these clouds and processes that are important in regulating cloud amount and cloud properties (e.g., Wyant et al. 1997; Moeng et al. 1996).

Despite major research efforts on marine stratocumulus, relatively little work has focused on continental stratus clouds (Del Genio et al. 1996; Sassen et al. 1999). Even though these clouds directly affect a relatively small area of the earth's surface compared with their marine counterparts, they affect local climate and weather and are linked closely to surface temperature and water budgets as well as the diurnal cycle. Changes in fractional cloudiness or other properties of continental stratus clouds may, in fact, explain a substantial portion of the observed increase in global temperatures during the last century due to a decrease in the diurnal cycle of surface temperatures over the continents (Karl et al. 1993). Despite their importance, even a basic description of continental stratocumulus and comparisons with their marine counterparts are severely lacking.

Studies of marine stratocumulus clouds have relied heavily on aircraft observations to define the turbulence fields in these clouds (e.g., Brost et al. 1982; Albrecht et al. 1985; Nicholls 1989). Measurements from tethered balloons have been used to define the turbulence structure in cloud-topped boundary layers (Hignett 1991; Caughey et al. 1982). Further investigations into the

Corresponding author address: Dr. Pavlos Kollias, Rosenstiel School of Marine and Atmospheric Sciences, University of Miami, Miami, FL 33149.
E-mail: pkollias@rsmas.miami.edu

© 2000 American Meteorological Society

Unauthenticated | Downloaded 04/21/24 11:41 PM UTC

turbulence structure of stratocumulus clouds have been made using large eddy simulation (LES) models (Moeng et al. 1992). This approach is becoming more attractive as models provide improved simulations of the cloud-topped boundary layer.

Millimeter-wavelength radars are among the new tools that have been developed during the past 10 yr for studying the properties of boundary layer clouds and the processes that affect those properties (e.g., Clothiaux et al. 1995; Miller and Albrecht 1995; Frisch et al. 1995a,b; Sassen and Liao 1996; Vali et al. 1998; Sassen et al. 1999). Observations from a 35-GHz radar operating from the island of Porto Santo during the Atlantic Stratocumulus Transition Experiment (ASTEX; 1992) have been used to describe the microphysical and turbulence structure of marine boundary layer clouds (Frisch et al. 1995a,b). These ASTEX studies indicate the utility of short-wavelength radars for describing the turbulence characteristics of a marine stratocumulus cloud. Vertical velocities from the radar provide a description of vertical structure of large eddies within the boundary layer that is difficult to define using in situ aircraft observations. Vali et al. (1998) studied the microphysical and turbulence structure of stratocumulus clouds off the coast of Oregon using an airborne 95-GHz radar as well as in situ observations made with the aircraft. These previous studies show that cloud observations obtained from short-wavelength radars provide vertical and horizontal resolution that is close to the resolution of LES models, thus indicating the possibility of direct comparison with these models.

In this study a 94-GHz (3-mm) Doppler radar is used to investigate the temporal evolution of the turbulent-scale vertical velocity field in a continental stratus cloud using the techniques of Frisch et al. (1995b). The mean structure of the cloud is further defined using a laser ceilometer to obtain cloud-base height and a microwave radiometer to measure the liquid water path. The scale and intensity of large eddy circulations in the cloud are defined from the vertical velocity analysis. Vertically coherent ascending and descending branches are identified and the vertical structure of these circulations is quantified. This analysis is used to examine the consistency of a mass-flux representation of the boundary layer turbulence structure described by Randall et al. (1992). Methods are developed to examine the relationship between entrainment processes and large eddy circulations in the cloud.

2. Instrumentation and data processing

The observations for this study were made from a suite of remote sensing systems operating from a site in central Pennsylvania. The principal observing system was a 94-GHz (3-mm wavelength) radar that provided cloud reflectivity and vertical velocity observations as a function of height using the pulse-pair technique. The radar is described by Clothiaux et al. (1995) and Peters et al. (1993) and is similar in design to the radar described by Lhermitte (1987). The transmitter peak power is 1.4 kW, and the system uses a bistatic antenna system with a beam width of 0.24° (about 4 m at a range of 1 km) for each antenna. For the observations in this study the radar was operated with a pulse repetition frequency of 10 000 Hz and a pulse width of 500 ns. The Doppler processor (Gray et al. 1989) uses a pulse-pair autocovariance algorithm (Lhermitte 1987), for calculating the mean Doppler velocity. The processor was configured to average 10 000 samples at 2-s intervals. The radar and processor settings give 28-m vertical sampling and unambiguous velocity range estimates of ± 8 m s^{-1}. The uncertainty in the estimated velocities is less than 5 cm s^{-1}. Calibration of the radar and data processing techniques are described in detail by Clothiaux et al. (1995).

A Vaisala laser ceilometer model (CT12K) located near the radar provided cloud-base heights with a vertical resolution of 15 m. The ceilometer uses a gallium arsenide semiconductor laser diode and provides cloud-base heights at 30-s intervals. A 50-MHz wind profiler provided hourly averaged wind speed and direction from 1 to 15 km above ground. A microwave radiometer (Han and Thomson 1994) with channels at 22.24 and 31.65 GHz, was used to retrieve liquid water content and integrated water vapor at 5-s intervals. All of the observing systems except the wind profiler were located at a site 10 km southwest of the Pennsylvania State University campus. This site is located in a wide valley with mountain ridges oriented southwest–northeast, separated by about 14 km, and rising to a height of about approximately 400 m above the valley. The wind profiler was operated from a site that was 10 km southeast of the main site. Standard surface meteorological observations were also available for the analysis.

The observations used in this study were obtained during a continental stratus experiment that was designed to study stratocumulus clouds that are frequently observed over the eastern United States. During the first phase of this experiment (15 October–15 December 1994) a variety of cloud structures were observed. The ceilometer, wind profiler, and microwave radiometer were operated continuously during this observing period. The radar was operated during periods when either low-level stratus or cirrus clouds were present over the site.

3. Meteorological conditions and macroscopic cloud properties

The observations used in this study were made on the 18 November during an 8-h period. Stratus clouds developed several hours prior to the observation period with cirrus and altostratus above. The stratus cloud deck was associated with southeasterly flow indirectly caused by Tropical Storm Gordon 800 km south of the site with high pressure centered at 1000 km to the northeast as

Unauthenticated | Downloaded 04/21/24 11:41 PM UTC

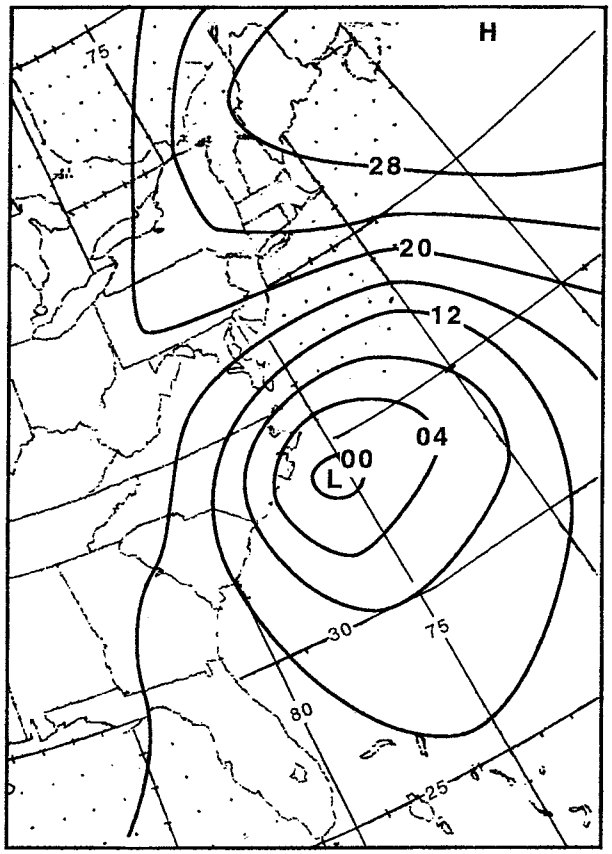

FIG. 1. Isopleths of 1000–500-mb thickness for 1200 UTC Nov 1994 where Tropical Storm Gordon is shown off the east coast of the United States.

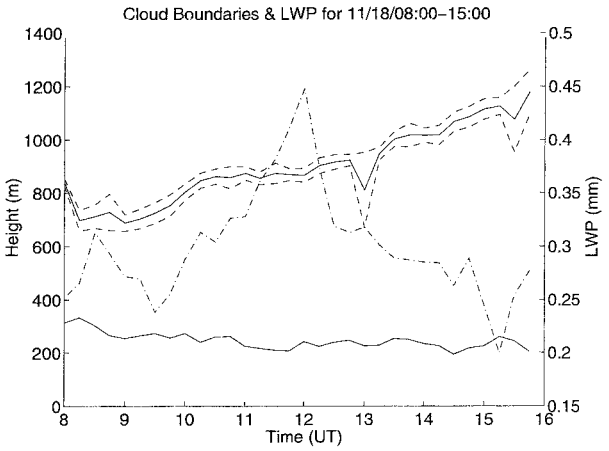

FIG. 3. Averaged values (15 min) of cloud base and top heights (solid lines) and cloud-top height standard deviation (dashed lines), and LWP (dot–dashed line).

shown by the surface pressure field (Fig. 1). Our analysis begins at 0800 UTC (0300 LST) after clouds above the boundary layer were diminished. The analysis extends through 1500 UTC (1000 LST) when the cloud structure became complicated and measurable precipitation was observed. During the 8-h observing period the temperature near the surface site increased from 10.5° to 13°C, and the relative humidity was near 96%–97%. The increasing temperature is consistent with warm advection associated with the southeasterly flow.

A series of 8, 1-h time–height cross sections of cloud reflectivity from the 94-GHz cloud radar provide a detailed mapping of the vertical cloud structure. Figure 2 shows the reflectivity mapping of the low-level stratus cloud for two hours: 0900–1000 and 1200–1300 UTC. The cloud bases from the ceilometer and cloud tops retrieved from the radar reflectivity using the technique developed by Clothiaux et al. (1995) are included. Averaged (15-min) values of cloud boundaries during the 8-h period (Fig. 3), show a relatively uniform cloud structure with a cloud top gradually ascending from 700 to 1100 m, and more steady cloud-base height varying

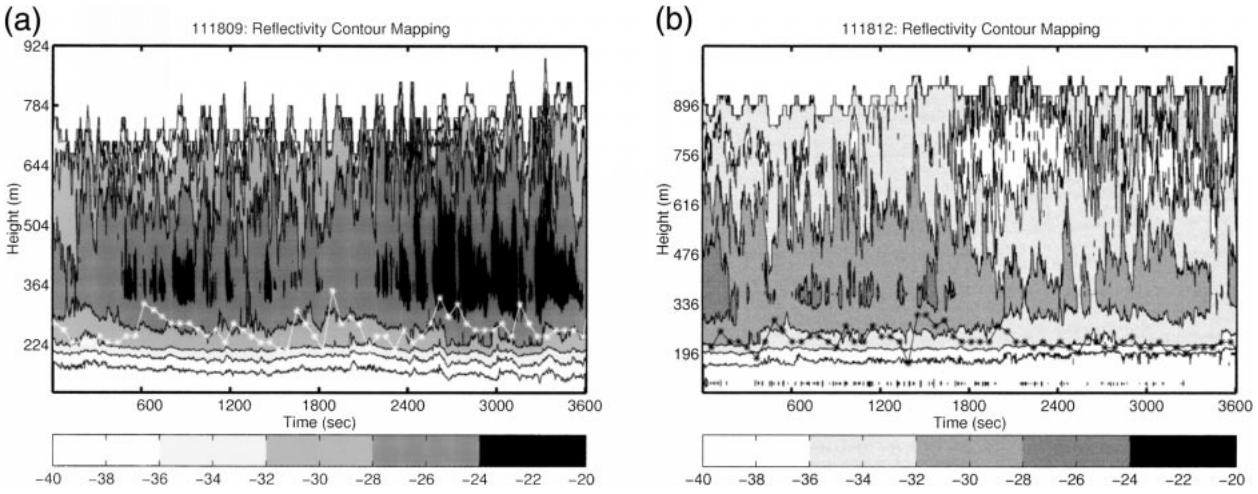

FIG. 2. Time–height cloud reflectivity from the 94-GHz radar for (a) 0900–1000 UTC. The white line is the cloud base from the ceilometer and (b) cloud reflectivity from 1200–1300 UTC. The black line is the cloud base from the ceilometer.

Unauthenticated | Downloaded 04/21/24 11:41 PM UTC

only between 220 and 300 m. The standard deviation of the cloud-top boundary shown in Fig. 3 was estimated by removing the linear trend for 15-min intervals and calculating the standard deviation for these intervals. The standard deviation is generally less than 40 m, indicating a fairly solid stratus cloud deck. The liquid water path (LWP) increases as the cloud depth increases during the first 4 h of the observing period. After 1200 UTC (0700 LCT), however, the LWP decreases despite the cloud depth continuing to increase. The differences in the character of the cloud during the first few hours of the observational period compared with those observed later are illustrated in the reflectivity structure in Figs. 2a,b. There is evidence of a two-layer structure associated with decoupling during the later part of the observing period as shown in Fig. 2b. This decoupling is consistent with the decrease in the LWP. The increase in the height of the capping inversion at cloud top may result from either weakening subsidence or the advection of higher inversion layers into the region. We will show later that the turbulence intensity, and thus the entrainment, weakens substantially with this decoupling. The mean wind speed at 1.2 km is estimated from the 50-MHz wind profiler to be approximately 10 m s^{-1} during the beginning of the observing period and decreasing to 6 m s^{-1} later in the observing period. At the surface, winds at 10-m height were 4 m s^{-1} at the beginning of the observing period and later decreased to 2.5 m s^{-1}. Winds were from the southeast at this level.

4. Drizzle effects on turbulence measurements

The presence of drizzle (droplets greater than 100 μm) in the sampling volume of the radar beam may induce a bias in the measurement of the air vertical velocity. Although drizzle droplets will move with the turbulent motion, if drizzle is systematically associated with either upward or downward motion, drizzle droplets may bias the turbulence statistics. Since the mean Doppler velocities were estimated using the pulse-pair autocovariance technique, no detailed information on the characteristics of the drizzle from Doppler spectra is available. Surface observers reported neither drizzle nor rain during the analysis period. However, using the reflectivity and Doppler velocity measurements, the influence of large drops in the estimate of the air vertical velocity can be estimated (Frisch et al. 1995b; Vali et al. 1998). Figure 4 shows the vertical profile of the correlation coefficient between the vertical velocities and the reflectivities from the 2-s radar observations from 1000 to 1100 UTC. In the lower part of the cloud there is a small negative correlation between reflectivity and velocity, indicating a possible but minimal influence of falling large droplets. However, in the upper two-thirds of the cloud layer the correlations are near zero, indicating that large drops have little effect on the velocity measurements. Furthermore, in the upper part of the stratocumulus, reflectivities are between −40 and −25 dBZ, values relatively low for large drops.

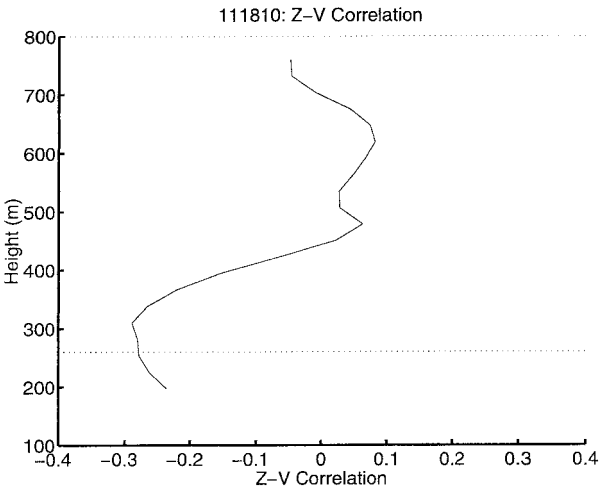

FIG 4. Vertical profile of the correlation coefficient between reflectivity and vertical velocity for 1000–1100 UTC.

Figure 5 shows the vertical velocity as a function of reflectivity at $\eta = 0.25$, where $\eta = (z - z_b)/(z_t - z_b)$ is the cloud normalized height and $\eta = 0.75$ from 1000 to 1100 UTC. The mean downward velocity in the lower part of the cloud layer reaches 0.5–0.7 m s^{-1}. Such velocities correspond to fall velocities of large droplets with sizes up to 200 μm if the mean air velocity is near zero. At $\eta = 0.75$ no dependence between reflectivity and vertical velocity exists. At $\eta = 0.25$, a small dependence at high reflectivities ranging from −22 to −12 dB*Z* can be seen. At the same level, but later in our period (1200–1300 UTC), the reflectivities near the cloud base are much weaker, ranging between −33 and −22 dB*Z* (Fig. 5c). For this later observing period the correlation between reflectivity and velocity is weak.

On average, the correlation between reflectivity and velocity in the lower part of the cloud was less than −0.2. In the upper part of the cloud layer it was close to zero, indicating that drizzle does not substantially affect the velocity measurements at this level. The shape of the correlation profile, negative in the lower part of the cloud and positive in the upper part, is similar to the reverse ''s'' pattern observed by Vali et al. (1998) in their coastal stratus study, but the correlations observed here are substantially less than in the coastal stratus where higher drizzle rates were observed. Further evidence that drizzle is having little impact on the turbulence is indicated by the spectral analysis shown in section 6c.

5. Turbulence statistics

a. Hourly analysis

The evolution of continental stratiform clouds depends to a large extent on the turbulence motions within

Unauthenticated | Downloaded 04/21/24 11:41 PM UTC

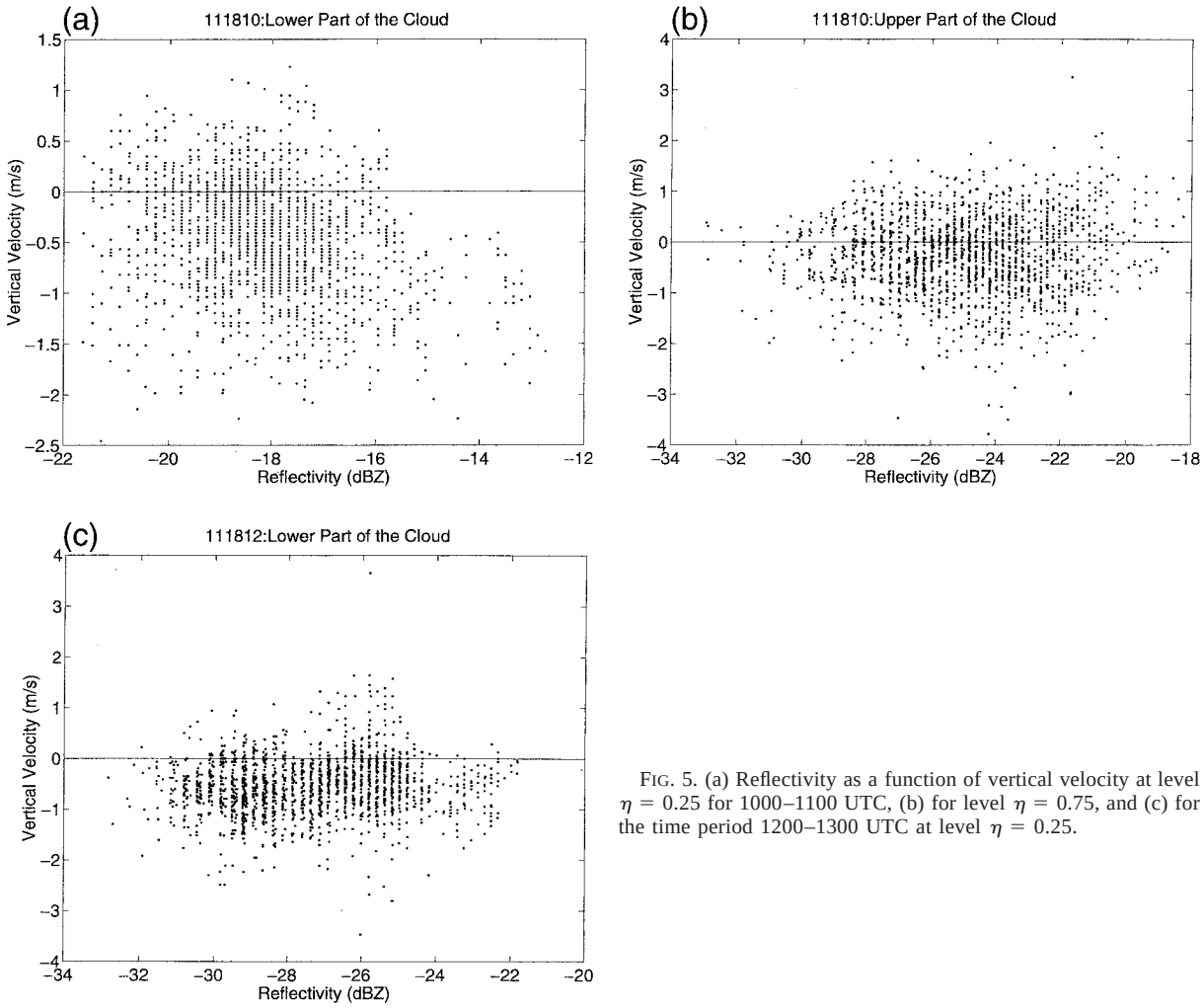

FIG. 5. (a) Reflectivity as a function of vertical velocity at level $\eta = 0.25$ for 1000–1100 UTC, (b) for level $\eta = 0.75$, and (c) for the time period 1200–1300 UTC at level $\eta = 0.25$.

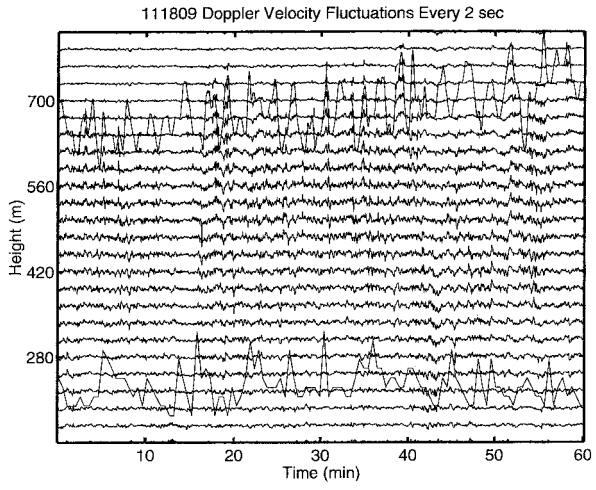

FIG. 6. Time–height section of the vertical velocity fluctuations for 0900–1000 UTC with cloud boundaries. (The velocity spans 6 m s^{-1} between gates.)

the clouds. The observations were made at night until late morning, a time when we expect a major source of energy for generating turbulence to be longwave radiative cooling at cloud top. In this section we examine the evolution of the turbulence structure during this observing period.

To remove any mean bias in the vertical velocities due to the fall velocities of the larger drops, the velocity deviations from successive 1-h means were calculated. Although the removal of the mean is not essential to the calculation of higher order moments, it aids in the identification of updraft and downdraft structures. In addition, the removal of the 1-h means filters out mesoscale vertical velocity variability and removes a vertical variation in the mean velocity that results from an increase in returns from large droplets at the lower levels in the cloud. The temporal and vertical distribution of the velocity perturbations is illustrated in Figs. 6–8 for 0900–1000 UTC (0400–0500 LCT), 1100–1200 UTC (0600–0700 LCT), and 1300–1400 UTC (0800–0900 LCT). All the gates within the cloud are shown along

Unauthenticated | Downloaded 04/21/24 11:41 PM UTC

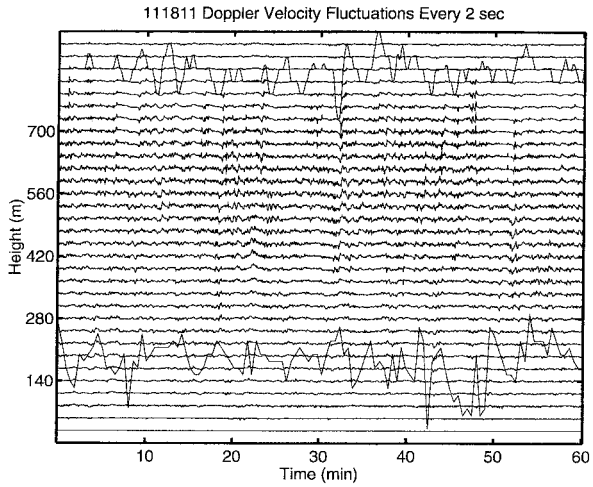

FIG. 7. Same as Fig. 6, but for 1100–1200 UTC.

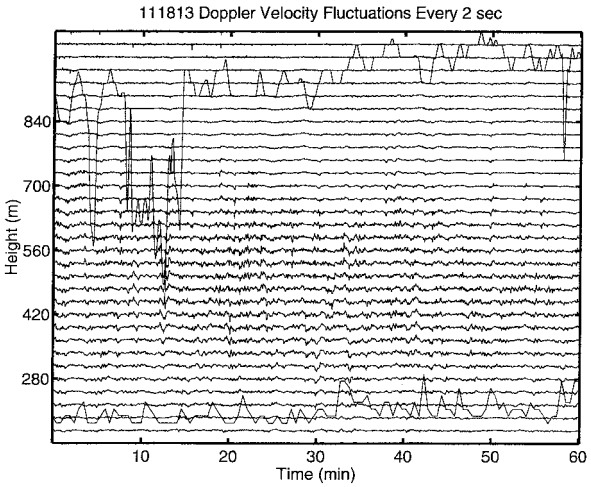

FIG. 8. Same as Fig. 6 but for 1300–1400 UTC.

with the cloud-base heights from the ceilometer and cloud-top heights obtained from an objective analysis of the radar reflectivites.

The vertical velocity fields shown in Fig. 6 during the first part of the period indicate well-defined updraft and downdraft structures. Some of these structures extend through the entire depth of the cloud. Most of the downdrafts appear to originate at cloud top where the cloud-top undulations have average amplitudes of about 40 m. A comparison of the vertical velocity fields observed during the nighttime period (0900–1000 UTC) with the morning periods (1100–1200 and 1300–1400 UTC) indicates a gradual shift of the updraft–downdraft activity from the upper part to the lower part of the cloud. During the later period the updrafts and downdrafts are less intense and have less vertical extent. The observations during this period are consistent with a decoupling between the cloud-top undulations and the downdraft and updraft structures observed in the lower part of the layer. The upper part of the cloud is relatively less turbulent in the later period. The cloud-top height, however, continues to vary with about the same amplitude as during the earlier part of the observing period. The mean wind speed near the cloud top is about 10, 8, and 6 m s^{-1}, respectively, during the three periods shown in Figs. 6–8.

During the 1300–1400 UTC period a discontinuity in the cloud top indicates a hole in the cloud associated with a downdraft that extends to the lower part of the cloud layer. The updrafts and downdrafts in this period are barely detectable in the upper part of the cloud indicating that the buoyancy generation mechanisms are substantially surpressed at the cloud top during this time. Although we cannot identify the source of energy for the penetrative downdrafts observed early in the period, it is possible that a buoyancy reversal due to entrainment may be involved. Unfortunately, a local sounding was not available to evaluate the thermodynamic structure associated with this cloud.

b. Analysis of variance and skewness

The average profiles of variance and skewness were computed by using the perturbation vertical velocities. We examine the temporal evolution of these statistics through the 8-h observing period. The vertical velocity variance is used as an indicator of turbulence activity and is plotted against normalized cloud height η for each of the hourly periods (Fig. 9). Each variance profile for the first 6 h of observations has a well-defined maximum. Although no vertical averaging was used, the vertical structure at 30-m resolution is relatively smooth. These variance profiles differ from the radar-derived profiles obtained by Frisch et al. (1995b) in a marine stratocomulus cloud observed over the island of Porto Santo during ASTEX where pronounced double peaks in the variance profile were observed both at night and during the day. Hignett (1991), using observations from a tethered balloon in the shallow marine stratocumulus cloud off the coast of California, found a decrease in the variance during the day, but the peak remained near cloud top both during the day and the night.

During the first 2 h of the observing period (0800–1000 UTC, 0300–0500 LCT), the maximum variance is found in the upper part of the cloud. The height of the maximum of the variance profile rises slightly from 0800 to 1000, possibly in response to the diminishing altostratus above the boundary layer clouds. This is consistent with the contribution of cloud-top radiative cooling on the buoyant production of turbulence. Additional factors, such as entrainment, wave activity, and wind shear may also contribute to the turbulence structure near the cloud top. Vigorous coherent velocity perturbations and their relationships with the cloud-top height fluctuations are illustrated in Fig. 6 and will be examined in more detail later in this manuscript.

Unauthenticated | Downloaded 04/21/24 11:41 PM UTC

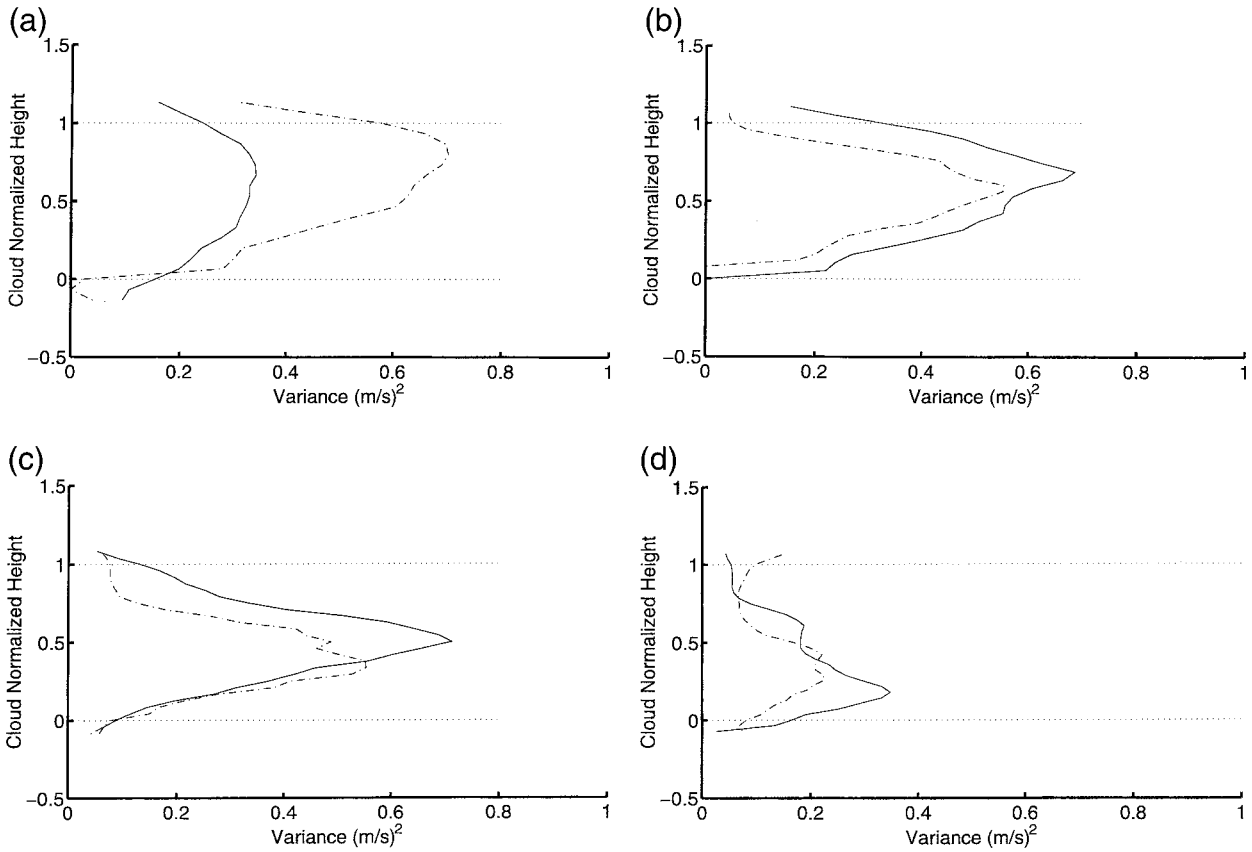

FIG. 9. Vertical velocity variances for (a) 0800–0900 (solid) and 0900–1000 UTC (dashed), (b) 1000–1100 (solid) and 1100–1200 UTC (dashed), (c) 1200–1300 (solid) and 1300–1400 UTC (dashed), and (d) 1400–1500 (solid) and 1500–1600 UTC (dashed).

The vertical velocity variance profiles evolve systematically with time. There is a gradual descent of the maximum in the variance, indicating that the intensive turbulence activity is also descending toward the lower part of the cloud. From 0900 to 1200 UTC the cloud-top height increased. At the same time, it is apparent from the time–height (t–z) mapping of the reflectivity (Fig. 2b) that in addition to the rise of cloud top, the upper part of the cloud becomes less reflective. This implies the formation of a stable layer that may limit the vertical extent of mixing and reduces transports between the upper and lower part of the cloud. This decoupling is consistent with the evolution of the variance profiles obtained for 1300 and 1400 UTC (Fig. 9) where there is some evidence of a double-peaked structure. Another explanation or possibility is that the solar heating increases after 1200 UTC, thus compensating the cloud-top radiative cooling at cloud top.

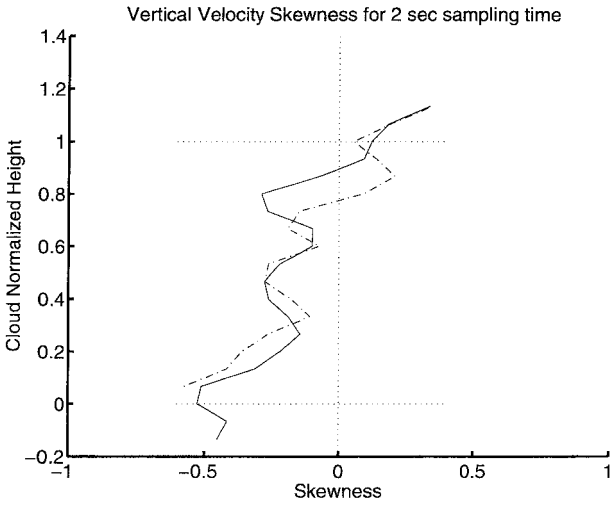

FIG. 10. Vertical velocity skewness for 0800–0900 (solid line) and 0900–1000 UTC (dashed line).

The turbulence structure was further characterized by evaluating the skewness S_w. The skewness provides a measure of the asymmetry in the distribution of vertical velocity fluctuations. Early in the observational period, when the turbulence activity is a maximum in the upper part of the cloud, S_w (Fig. 10) is positive in the uppermost part of the cloud and negative in the lower part of the layer. The positive skewness is most likely due to a few strong updrafts extending to and impinging upon the stable layer at cloud top. The impinging updrafts lose their kinetic energy at the inversion, thus S_w

Unauthenticated | Downloaded 04/21/24 11:41 PM UTC

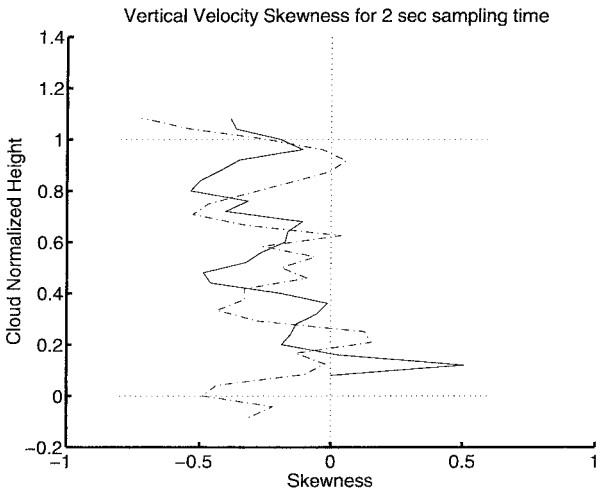

FIG. 11. Vertical velocity skewness for 1000–1100 (solid line) and 1100–1200 UTC (dashed line).

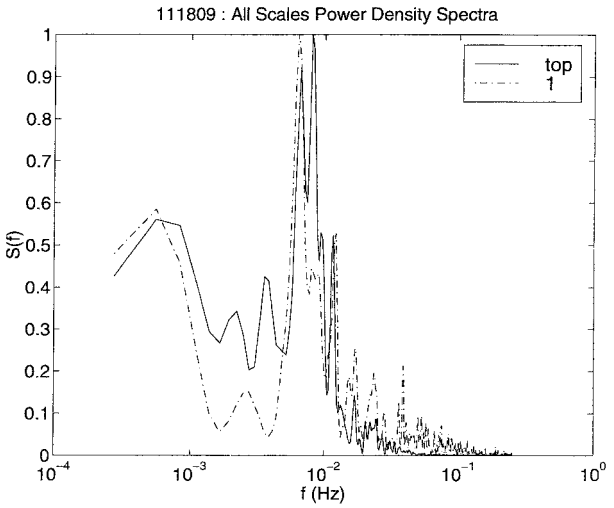

FIG. 12. Spectra of cloud-top height and vertical velocity at cloud top 0900–1000 UTC.

further increases with height within the inversion layer (Moeng and Rotunno 1990). When cloudy and clear air mix in the entrainment zone the mixture may experience evaporative cooling and with the aid of radiative cooling can give rise to negatively buoyant parcels. These mixtures may then be accelerated downward into the cloud deck as cold downdrafts that cause negative skewness in the lower levels. Such a vertical profile of skewness, positive in the upper part and negative in the lower part of the cloudy layer, is consistent with numerical simulations of stratus-topped boundary layer driven by cloud-top cooling and surface heating (Moeng 1986). The situation changes, however, during the period 1000–1200 UTC, where the vertical velocity skewness is negative throughout the cloud layer (Fig. 11). This vertical velocity skewness profile is consistent with LES of stratus-topped boundary layer driven by radiative cooling and with the majority of the in situ observations of nocturnal stratocumulus (e.g., Moyer and Young 1991). LeMone (1990) suggests that the variability in the skewness profiles may be, in part, due to the presence of mesoscale quasi-two-dimensional structures within the PBL. This possibility will be further examined using a spectral analysis of the turbulent structure. In any case, it may not be valid to make detailed comparisons of the skewness with that from previous studies since the agreement depends on the closeness of the conditions used for the simulation to those under which the observations were taken. Finally, later in our observing period when the turbulence intensity diminishes, the S_w profiles (not shown here) show a relatively complicated structure.

c. Spectra analysis

Vertical velocity power spectra are calculated throughout the period at different normalized cloud layer depth. The 1-h segments of vertical velocity are used to construct the power spectra. Selected levels near the cloud top ($\eta = 1$), cloud base ($\eta = 0$), and $\eta = 0.25$, 0.5, and 0.75 for each hour were used to study the temporal variability of the vertical velocity power spectra. In addition, spectral analyses of the cloud-top heights were made. The cloud-top variability may result from a combination of wave and buoyancy activity. Early in the observing period (0900–1000 UTC, 0400–0500 LCT), a spectral analysis of the cloud-top boundary time series (Fig. 12) indicates a component of variability at a frequency of 5×10^{-4} Hz (equivalent to a period of 30–35 min) that is apparent in all levels throughout the cloud layer. Since the spectra reported here are at a fixed point, we apply Taylor's hypothesis to convert frequencies to estimates of wavenumbers by assuming a mean horizontal wind speed of 8 m s^{-1}. The observed peak corresponds to a horizontal scale of about 16 km. Such large scales may not be important for the in-cloud processes, but rather a manifestation of mesoscale variability and possibly wave activity. A second peak at intermediate frequencies is apparent throughout the layer and indicates that both mesoscale forcing and turbulence are present (Zhou et al. 1985). However, the turbulent component is the dominant source of the observed vertical velocity variability. Since our focus is on the smaller scales, the lower-frequency peak is not considered in the detailed spectral analyses shown below.

The dominant source of the observed cloud-top height variability at shorter wavelengths is at frequencies centered around 8×10^{-3} Hz (Fig. 13). This frequency peak for the cloud-top height corresponds to a scale of about 1 km and reflects motions at the scale of the major updrafts and downdrafts observed during the same period. The possibility of a breakdown of the cloud-top interface due to the development of Kelvin–Helmoholtz

Unauthenticated | Downloaded 04/21/24 11:41 PM UTC

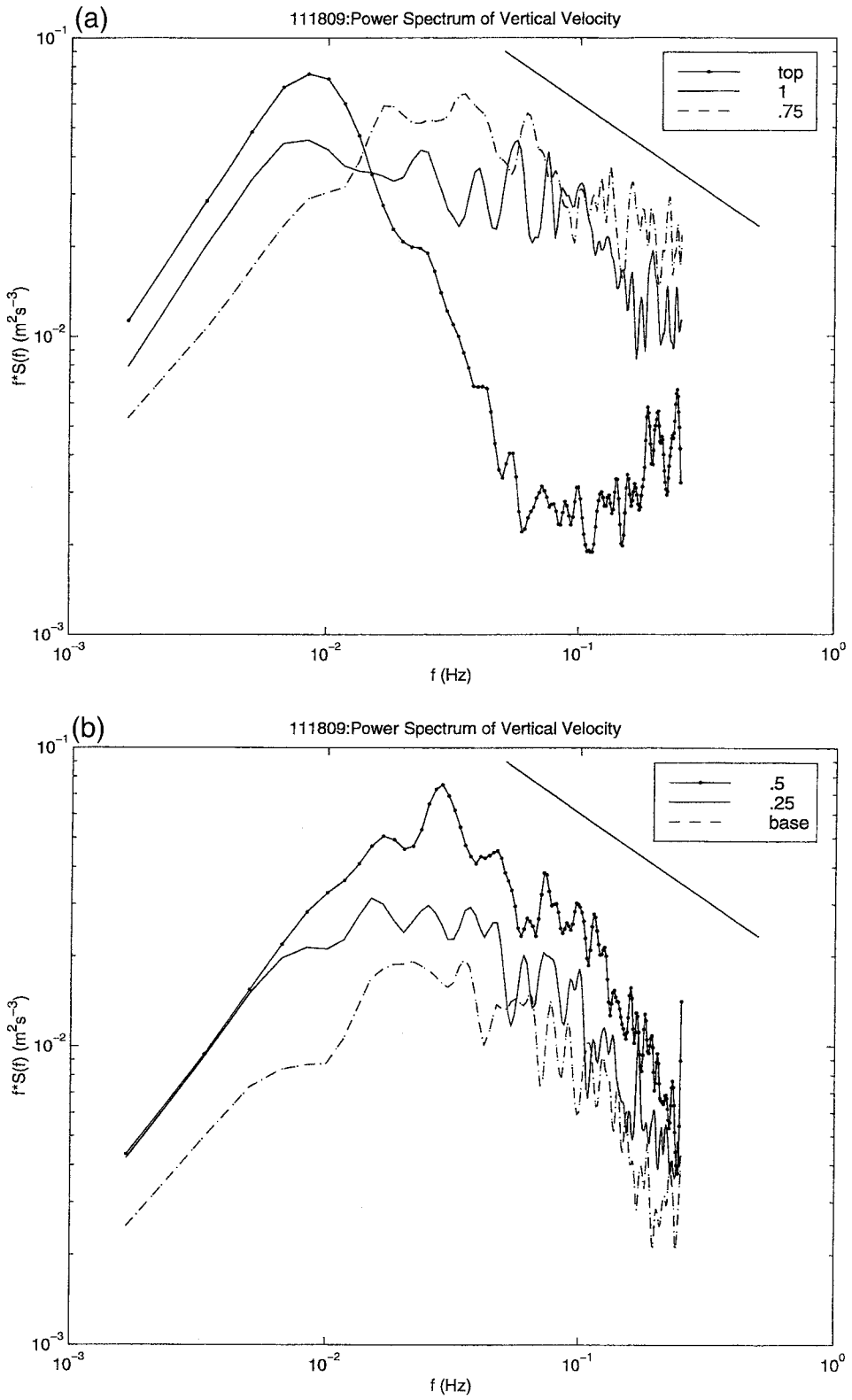

FIG. 13. Spectra of cloud-top height and vertical velocity spectra at selected levels η within the cloud layer for 0900–1000 UTC (straight line shows $-\frac{2}{3}$ slope) for (a) cloud-top height, vertical velocity at $\eta = 1$ and 0.75, and (b) $\eta = 0.5$, 0.25, and 0.0.

Unauthenticated | Downloaded 04/21/24 11:41 PM UTC

instability should be considered. Unfortunately, we are unable to obtain usable wind shear data across the cloud top using the 50-MHz wind profiler since the lowest gate is above the cloud top and the vertical resolution is quite coarse.

Figure 13 shows spectra of the vertical velocity at normalized heights of $\eta = 0.0$ (cloud base), 0.25, 0.5, 0.75, and 1.0 (cloud top). The vertical velocity spectrum near cloud top is similar to the spectrum of cloud-top height, consistent with a coupling between cloud-top interface variability and the vertical velocity near the cloud top. At the cloud-top level there are, however, significant spectral peaks at higher frequencies that correspond to horizontal scales between 100 and 400 m; variability at these scales becomes more apparent at lower levels in the cloud. From $\eta = 0.75$ to the cloud base these convective updraft and downdraft features dominate the spectra, although the energy associated with these scales decreases toward cloud base. A characteristic maximum wavelength is very difficult to identify. It is however, possible to identify a broad range of frequencies corresponding to horizontal scales between 100 and 400 m that contribute substantially to the variance. The envelope of the maximum variability is shifted slightly to higher frequencies in the lower part of the cloud layer. Such a shift is consistent with the turbulence being driven by buoyancy processes near cloud top. During the 1200–1300 UTC (0700–0800 LCT) period, the spectra of cloud-top height and vertical velocities in the upper part of the cloud (Fig. 14a) indicate substantially less variability at scales in the 100–400-m range than observed earlier in the observing period. In the middle to lower part of the cloud, there is still substantial variability at these scales of motion. At higher frequencies, portions of the spectra have a slope close to $-\frac{2}{3}$, although the slope tends to be greater than this at levels in the cloud where the 100–400-m scale motions are enhanced.

d. Conditional sampling and mass-flux representations

A cloud mass-flux representation of the vertical turbulent fluxes can provide a physical framework for understanding and parameterizing the effects of shallow convection in maintaining the vertical structure of the boundary layer (Wang and Albrecht 1986). This approach is based on the assumption that coherent updrafts and downdraft structures are responsible for a substantial fraction of the vertical transport. The mass-flux representation in stratocumulus has been evaluated using aircraft observations (e.g., Penc and Albrecht 1987) and results from LES (e.g., Randall et al. 1992). In these approaches conditional sampling techniques are used to identify updraft and downdrafts (e.g., Jenson and Lenschow 1978; Lenschow and Stephens 1980; Wang and Albrecht 1994). A fundamental parameter of the mass-flux approach is σ the fractional area covered by rising branches of convective cells or updrafts. The radar observations in this study allow for a detailed mapping of the vertical velocity field and a direct sampling of the structure of updrafts and downdrafts identified using either just the sign of the vertical velocity fluctuations or the strength and vertical coherence of the structures. In addition, the radar observations of w can be used to evaluate the technique described by Randall et al. (1992, hereafter referred to as R92) to relate σ and the mass-flux M_c to turbulence statistics. In this technique, a ''top-hat'' representation of updraft and downdraft properties is used to express the first three moments of the vertical velocity as functions of σ, w_u, and w_d, where w is vertical velocity and u and d indicate upward and downward motions. Following the formulation of R92 the area average of w is given as

$$\overline{w} = w_u\sigma + w_d(1 - \sigma). \tag{1}$$

The variance is given as

$$\begin{aligned}\overline{w'^2} &= \sigma(w_u - \overline{w})^2 + (1 - \sigma)(w_d - \overline{w})^2 \\ &= \sigma(1 - \sigma)(w_u - w_d)^2 \end{aligned} \tag{2}$$

and the skewness is given as

$$\begin{aligned}\overline{w'^3} &= \sigma(w_u - \overline{w})^3 + (1 - \sigma)(w_d - \overline{w})^3 \\ &= \sigma(1 - \sigma)(1 - 2\sigma)(w_u - w_d)^3. \end{aligned} \tag{3}$$

Equations (1)–(3) can be solved for the three unknowns σ, w_u, and w_d. Furthermore, the mass-flux M_c is given by

$$M_c = \rho\sigma(1 - \sigma)(w_u - w_d). \tag{4}$$

As shown by R92 the solution of the set of Eqs. (1)–(3), is

$$\sigma = \frac{1}{2} - \frac{S_w}{2\sqrt{4 + S_w^2}}, \tag{5}$$

where

$$S_w = \frac{\overline{w'^3}}{(\overline{w'^2})^{3/2}}, \tag{6}$$

and the convective mass flux is given by

$$M_c = \frac{\rho\sqrt{\overline{w'^2}}}{\sqrt{4 + S_w^2}}. \tag{7}$$

The above set of equations is a complete set of equations for the determination of the fractional area covered by updrafts, the convective mass flux, and the vertical profiles of updraft and downdraft from an observed field of vertical velocity or a field simulated by an LES.

Two conditional sampling method strategies are applied to the dataset. The first is direct sampling based on the vertical velocity sign and the second adds a constraint of vertical coherency within the structure to identify updrafts and downdrafts. In this second method, coherent structures are identified by an upward vertical

Unauthenticated | Downloaded 04/21/24 11:41 PM UTC

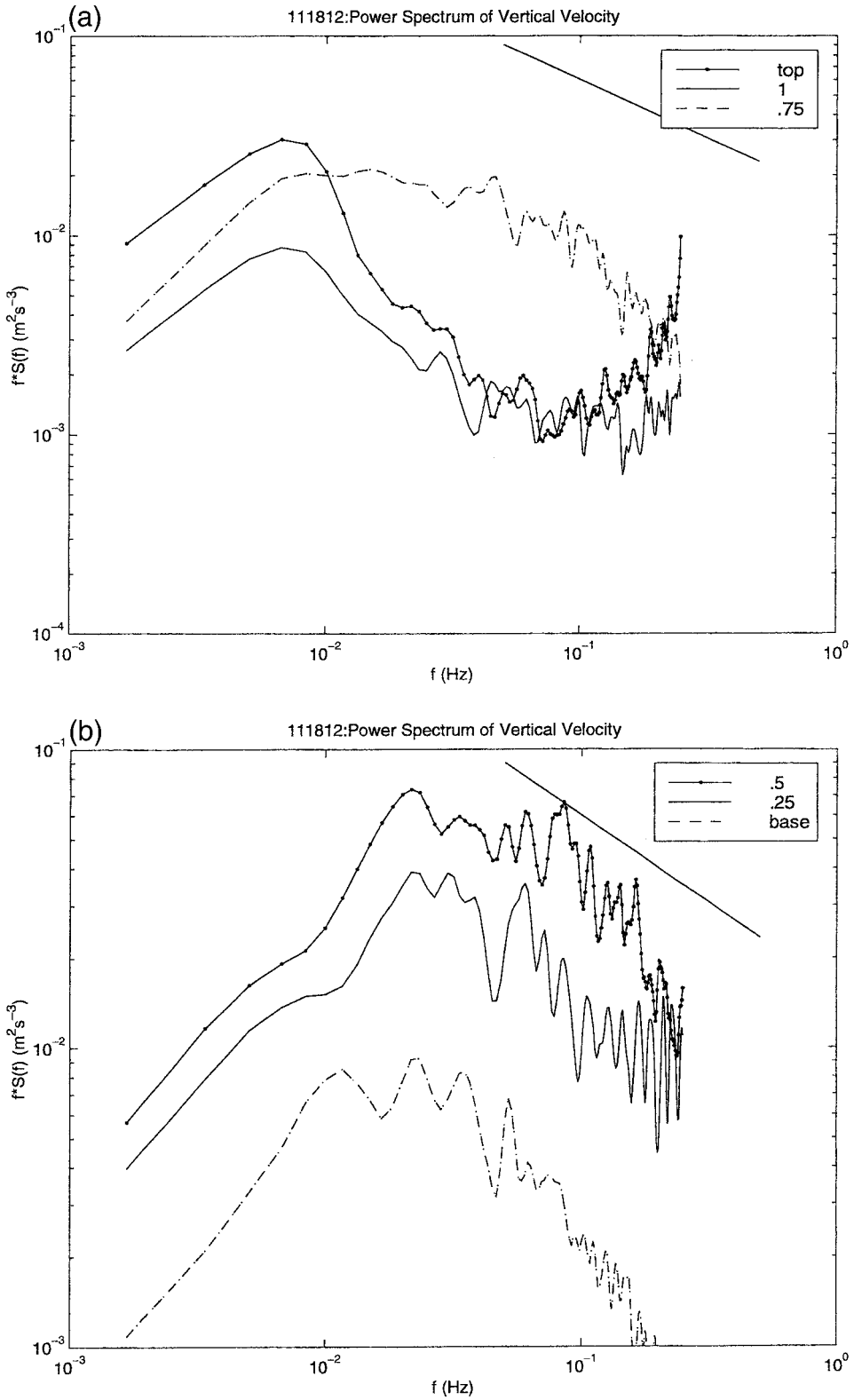

FIG. 14. Same as Fig. 13 but for 1200–1300 UTC.

Unauthenticated | Downloaded 04/21/24 11:41 PM UTC

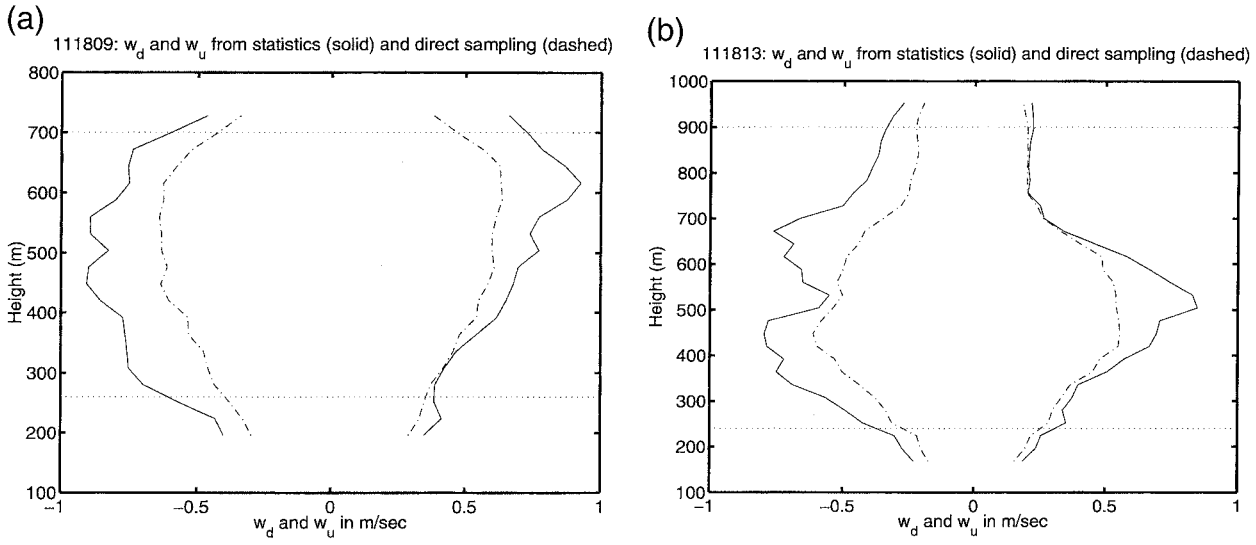

FIG. 15. The vertical profile of w_u and w_d obtained from statistics (solid lines) and by direct sampling of the observed field (dot–dashed lines) for (a) 0900–1000 UTC and (b) 1300–1400 UTC.

velocity observation in at least four adjacent gates (112 m). The first sampling technique is the classic plume decomposition of the flow and the second will be called a coherent decomposition. Both conditional sampling techniques are based on the sign of the vertical velocity. More restrictive decomposition techniques were also applied by specifying velocity thresholds in addition to the vertical coherency constraint.

The vertical profiles of w_u and w_d were estimated from the profiles of the statistical moments of the vertical velocity field by the method described by R92 for the 0900–1000 and 1300–1400 UTC observing periods. These values were compared with w_u and w_d by direct conditional sampling of w using the vertical velocity as an indicator (Fig. 15). The profiles from the two techniques are similar, but as found by R92 using LES vertical velocities, the statistical method overestimates the magnitude of the average upward and downward profiles relative to the direct sampling. The magnitude and the vertical distributions of σ and M_c for the 0900 profiles are shown in Fig. 16. The statistical method overestimates these parameters relative to direct sampling, although the profiles have the same behavior in the vertical as shown in R92. Analyses of all eight 1-h segments show similar results. The mass flux (assuming $\rho = 1$ kg m^{-3}) shown in Fig. 16 for 0900–1000 UTC has a maximum of 0.3 kg m^{-2} s^{-1} in the upper part of the cloud layer where the maximum variance is observed. The fractional area covered by updrafts is close to 0.5, which is consistent with previous observations of stra-

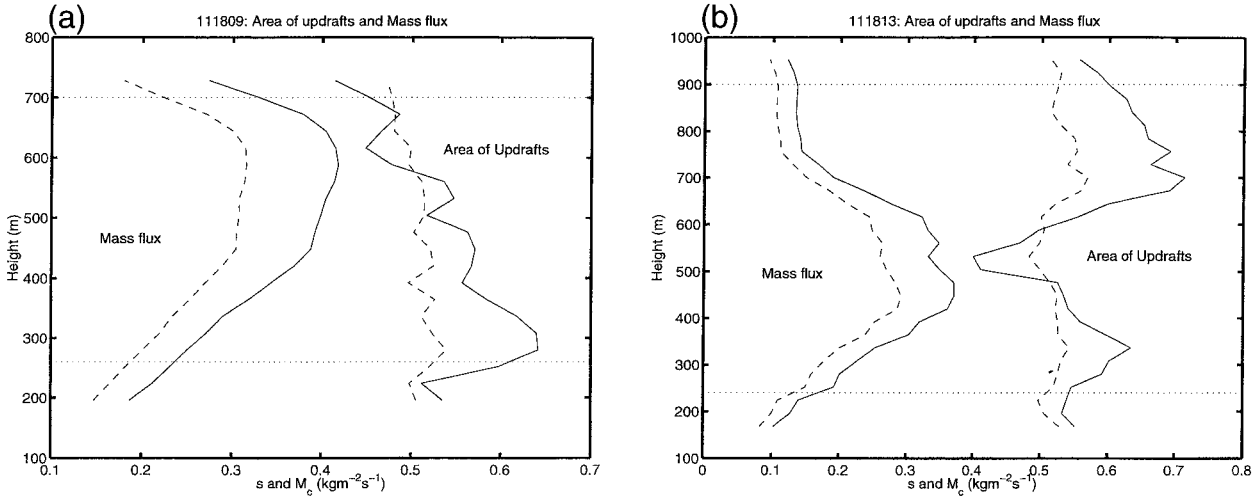

FIG. 16. The vertical profiles of σ and M_c from statistical method (solid) and by direct sampling (dashed) of the observed field for (a) 0900–1000 UTC and (b) 1300–1400 UTC.

Unauthenticated | Downloaded 04/21/24 11:41 PM UTC

tocumulus. The fractional coverage is slightly above 0.5 near the cloud base and below 0.5 near the cloud top. This case is offered for direct comparison with the third-order statistics produced by LES, since one of the ambiguities with the third-order statistics produced by LES models is the positive skewness in the upper part of the PBL. The dataset used here indicates that the radar provides a detailed mapping of the vertical velocity field in boundary layer clouds that can be used for direct comparison with LES results (Wang and Stevens 2000).

Components of the mass-flux description of the boundary layer for a 1-h period (1300–1400 UTC) during the decoupled phase of the cloud are shown in Figs. 15b and 16b. The upper 200 m of the stratocumulus is ''quiet'' with a very small mass flux despite large values of σ (Fig. 16b). This is due to the very small values of w_u (0.2–0.25 m s^{-1}). The maximum of the mass flux is located at the lower one-third of the cloud despite the small σ values there. The decoupling case and its complex structure with a solid cloud layer in the lower part and a shallow one above 500 m is used to further explore the R92 techniques. The statistical method and the direct sampling method are shown in Fig. 16b. The strong dependence of the statistical method on the skewness is apparent from the sharp shift of the fractional covered just above the internal cloud interface at 500 m. Here σ is less than 0.5 when the skewness is positive and more than 0.5 when the skewness is negative. Since the mass flux from the statistical method depends on the variance, there is an interesting double peak in the decoupled cloud. The direct sampling technique (Fig. 16b) shows a weaker double-peak structure above and below the internal interface.

The fractional area covered by updrafts and the associated mass flux was calculated using different thresholds on the vertical velocity (Fig. 17). The mass flux and the fractional coverage associated with the more intense updrafts have a pronounced peak at 600 m with little contribution in the lower levels. The mass flux and fractional area coverage of downdrafts greater than 1 m s^{-1} (not shown) have a maximum at 450 m compared with a maximum at 600 m for the updrafts. For the decoupled conditions at 1300 UTC shown in Fig. 17b, the fractional area covered and the mass flux of the updrafts have a maximum much lower in the cloud layer than for the coupled case. The double peak in the mass flux obtained from the statistics is reflected in the double-peak structure for the strongest updrafts, which is further reflected in the double-peak structure of the vertical velocity variance profile for the same period (Fig. 5).

6. Updraft–downdraft structures

a. Convective-scale structures

Early inferences about entrainment and cloud turbulence mainly relied upon thermodynamic measurements of temperature, liquid water content, and tracers like ozone (Wang and Albrecht 1986). The application of a ground-based 3-mm wavelength radar can provide substantial insight on the entrainment process by mapping the cloud structure from vertical velocity and reflectivity measurements.

To gain further insight into the detailed structure of these coherent updrafts and downdrafts, we plot time–height cross sections at two selected times within the cloud. The first is a 4-min period during the nighttime from 0915:50 to 0919:50 UTC. The updraft and downdraft structures in this case are clearly defined in Fig. 18a. During this observing period two cloud-top peaks with mean amplitudes of about 50 m are observed. It is apparent that the front (downshear) part of the peaks is occupied by coherent downdraft structures, while the back (upshear) parts of the peaks are associated with updraft structures. Furthermore, the downdraft structures appear to originate at the cloud top and penetrate more than 300 m to the lower part of the cloud. The updraft structures tend to be more narrow and discrete than the downdrafts, especially near the cloud top. These smaller-scale updrafts perturb the cloud-top interface and tend to become narrower and weaker as they encounter a more stable stratification near cloud top. This results in a sharp velocity gradient at the upper part of the updrafts. The updraft cores tend to be slightly weaker than the downdrafts. The observations are consistent with the positive skewness values at the upper cloudy layer during the same period.

To further explore how the downdraft structures may relate to cloud-top entrainment, the entrainment zone is defined using the cloud-top reflectivity. In Fig. 18b, we plot dBZ contours near the cloud-top boundary for the same time segment along with the LWP from the microwave radiometer. If we define the entrainment zone to be associated with reflectivites between -31 and -40 dBZ, there is a strong coherence between the penetration of the entrainment zone into the cloud layer and the downdraft structures. The selection of the range of dBZ between -31 and -40 as entrainment zone is justified from the mean reflectivity profile at the same hour and from the reflectivity mapping at the same period (Fig. 2a). The -40 dBZ contour overlaps the cloud boundary for most of the period, and reflectivity values as high as -31 dBZ are very close to the cloud top, indicating that a sharp decrease in the reflectivity exists in a narrow region just below the cloud top. A 9-dBZ difference in reflectivity can be associated with a decrease of the number concentration of the cloud droplets by a factor of 8, a decrease of the mean (reflectivity weighted) droplet diameter by $\approx$40%, or some combination of both. The effect of the updrafts and downdrafts on the depth of the entrainment zone is consistent. In areas of downdrafts there is notable penetration of lower reflectivities into the cloud. This decrease in reflectivity is consistent with downdrafts diluted by the entrainment of drier air at cloud top. In

Unauthenticated | Downloaded 04/21/24 11:41 PM UTC

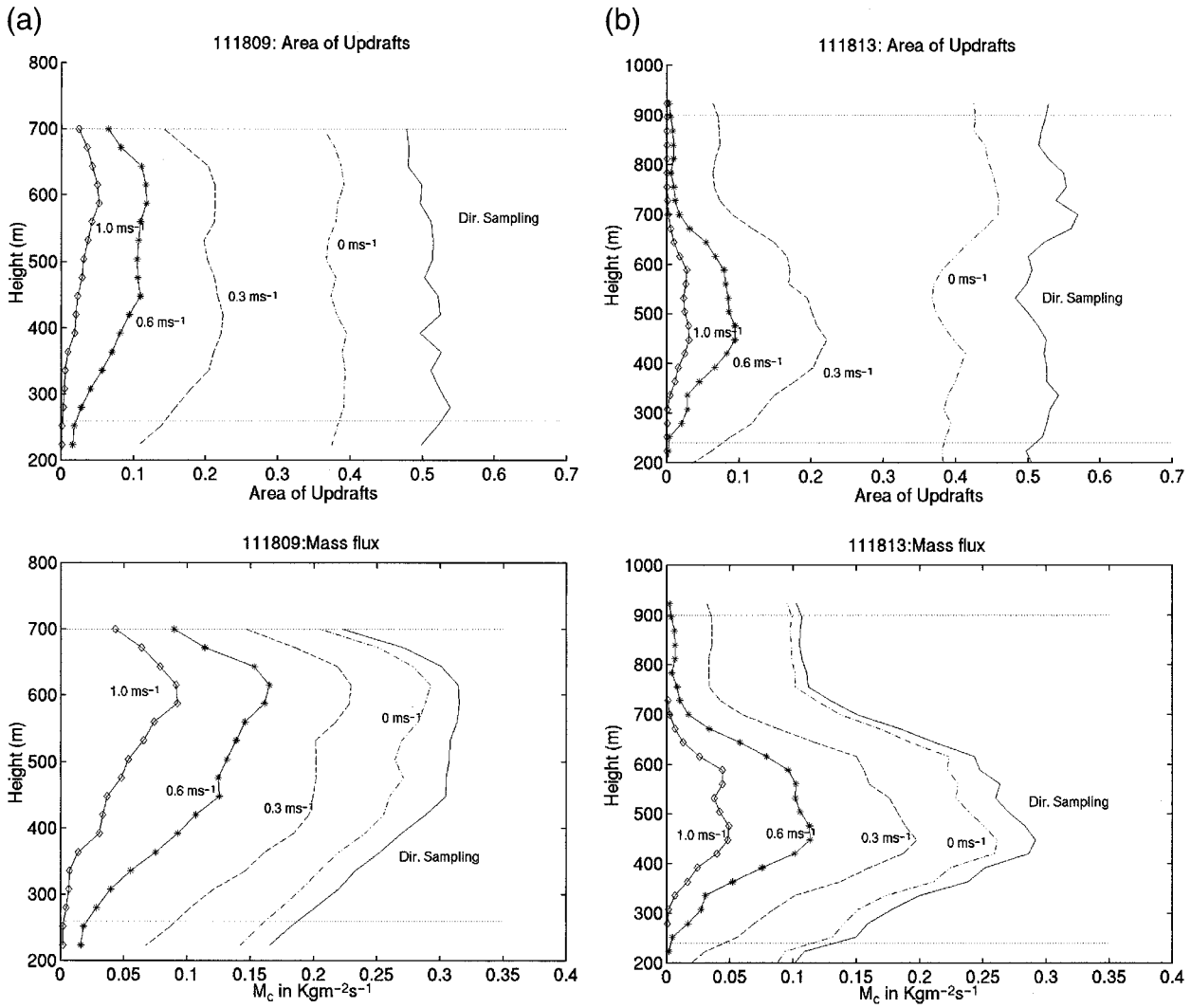

FIG. 17. Fractional area of updrafts and mass-flux profiles calculated using coherent structure sampling techniques with different positive velocity thresholding (solid line is direct sampling, dot–dashed line coherent sampling with 0 m s^{-1} thresholding, dashed line coherent sampling with 0.3 m s^{-1} thresholding, solid line with stars coherent sampling with 0.6 m s^{-1} thresholding, and solid line with diamonds coherent sampling with 1 m s^{-1} thresholding (a) for 0900–1000 UTC and (b) for 1300–1400 UTC.

areas of downdraft, the entrainment zone is about 100 m wide. In the rear part of the peak where the overshooting updrafts penetrate the inversion layer, the entrainment zone is defined by a sharper d*BZ* gradient and is decreased in thickness to less than 50 m. Such a coherent pattern of updrafts and downdrafts is consistent with the observations in fair weather cumulus of Kitchen and Caughey (1981) in a sheared environment. They observed that the updrafts overturn at cloud top in the direction of the mean wind shear, producing an inverted *P* structure.

Several other cloud-top peaks were analyzed during the same period (0900–1000 UTC). All these peaks show the same pattern described above. Figure 19 shows a time segment for 0950:10–0956:30 UTC. Although the separation between the downdrafts and updrafts is not as clear as it was in the first time segment, the same eddy structure is apparent. There is a marked vertical coherence between the up- and downdraft structures and the undulations apparent in the cloud-top interface early in our period. Figure 19a shows updraft and downdraft structures that extend through the whole cloud layer. As in the previous case, the downward penetrating areas of low reflectivity tend to be collocated with downdrafts. The LWP indicates that despite the thinning of the cloud, the LPW increases. This substantial LWP increase is associated with the broad area of updrafts and the production of liquid water due to condensation. On the other hand, the LWP tends to decrease in downdraft areas. This remarkable variability of the LWP on such small scales indicates the importance of the internal circulations on cloud microphysics.

Unauthenticated | Downloaded 04/21/24 11:41 PM UTC

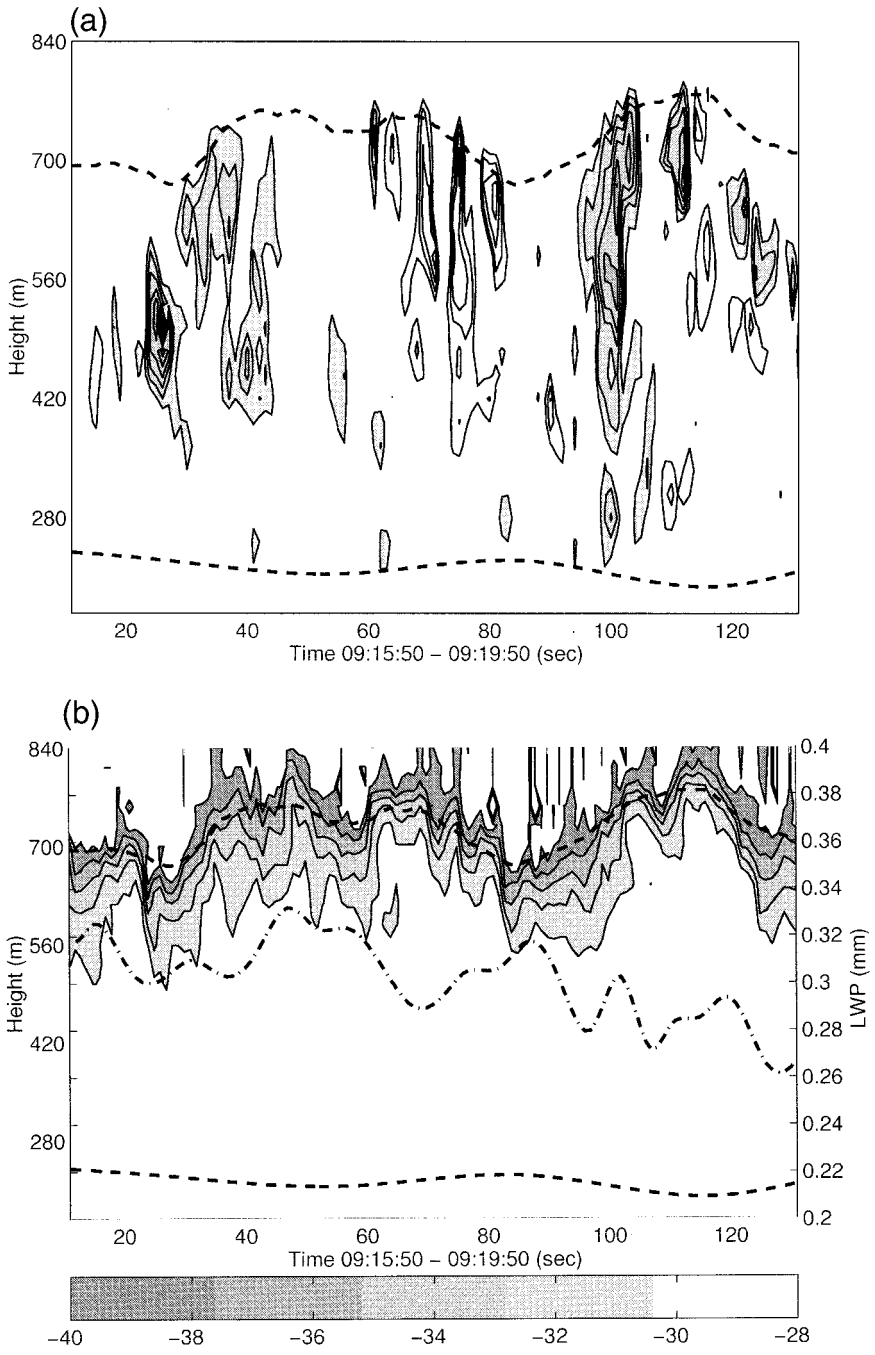

FIG. 18. (a) Detailed view of the vertical velocity contour for a small segment of observations (0915:50–0919:50 UTC) where the downdraft structures are shaded. The updrafts and downdrafts with absolute velocities more than 1 m s^{-1} are shown and the contours are plotted with 0.5 m s^{-1} interval. The cloud boundaries are also shown. (b) Radar reflectivity contour from −31 to −40 dB*Z* near the cloud top, where the cloud boundaries are also shown. The dot–dashed line is the LWP for the same period.

Both updrafts and downdrafts in these detailed mappings have an average width of 100–400 m and maximum absolute eddy-core velocities greater than 2 m s^{-1}. On several occasions the penetrative downdrafts reached the cloud base, indicating the importance of vertically coherent eddies. Although the general updraft and downdraft areas correspond to the 1-km horizontal variations in the cloud-top height, the cores within these regions have a much smaller horizontal extent. The inhomogeneity within the updraft regime is similar to that

Unauthenticated | Downloaded 04/21/24 11:41 PM UTC

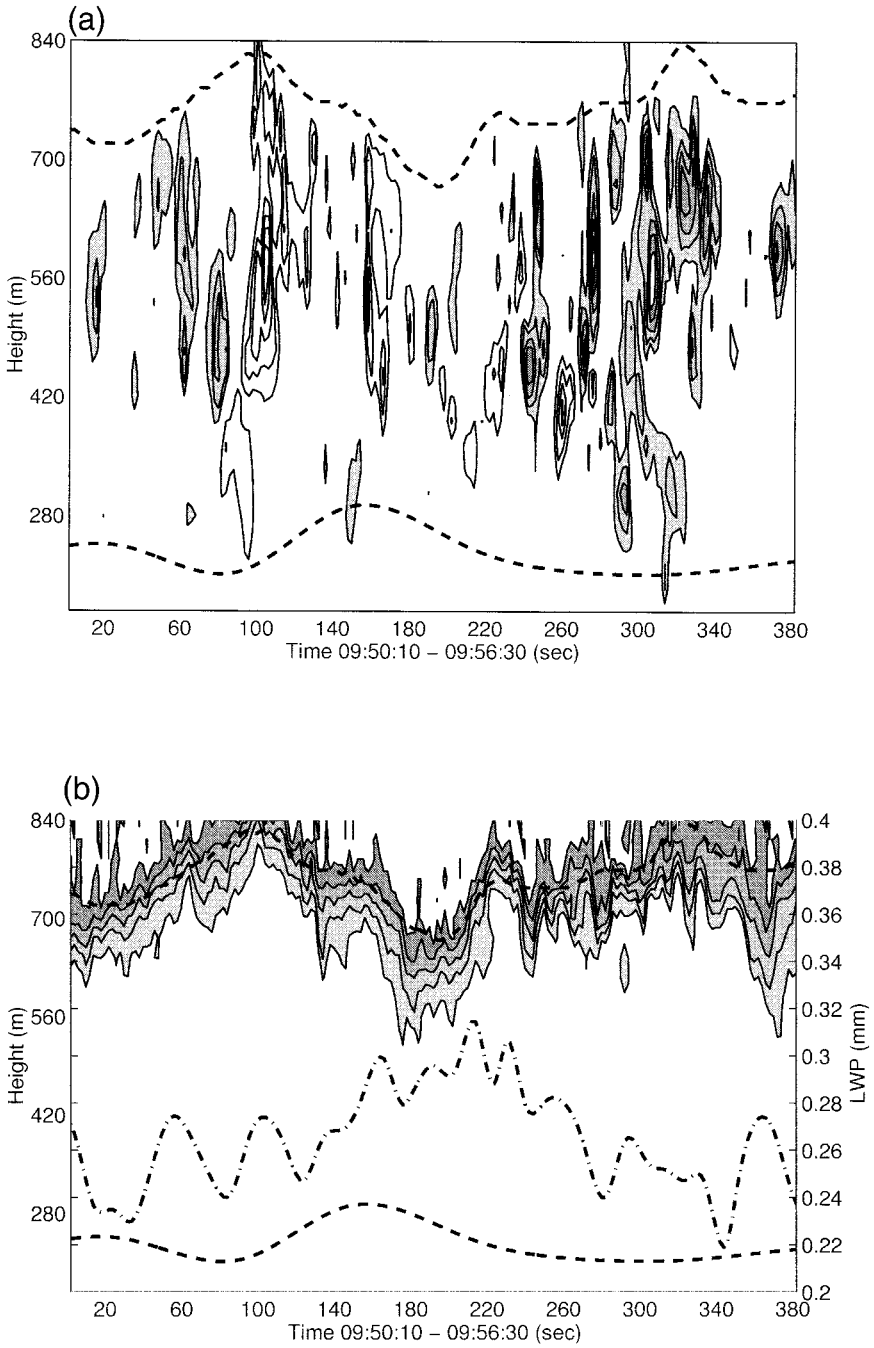

FIG. 19. Same as Fig. 18 but for 0950:10–0956:30 UTC.

sometimes observed from aircraft observations in fair weather cumulus clouds (Warner 1977).

7. Summary

This radar study of continental stratocumulus provides a detailed comparison of the vertical velocity statistics and macroscopic cloud properties for coupled and decoupled boundary layer conditions during an 8-h observing period. The high resolution continuous vertical velocity measurements used in this study illustrate the utility of a millimeter-wavelength Doppler cloud radar for tracing the time evolution of the turbulence structure in stratocumulus clouds. Although the radar observations have high vertical resolution, the profiles of the vertical velocity statistics are not noisy. In this study there was a substantial increase in the vertical velocity variance as a cloud layer (altostratus) above the bound-

Unauthenticated | Downloaded 04/21/24 11:41 PM UTC

ary layer stratocumulus was diminished during the first hour of the observing period. The variance maximum was elevated to near cloud top and then systematically descends (Fig. 9) during the final 6 h of the observing period. The descent of the vertical velocity variance maximum during later hours (but still prior to sunrise) reflects a decrease in turbulence at cloud top and the gradual formation of a stable layer within the cloud as indicated by a layer of decreased reflectivity. The height of the maximum variance in the turbulence tracks the movement of the internal reflectivity minimum that gradually descends through the cloud.

Although it is difficult to analyze and separate the contribution of the various mechanisms (entrainment, cloud-top radiative cooling, and wave-breaking activity at the interface) that may be operating in this cloud, the observed structures do indicate the nature of the relevant processes. Early in the observing period some of the downdrafts that originate near cloud top extend through the entire layer. This is consistent with the generation of negative buoyancy due to radiative cooling or possibly the entrainment and subsequent mixing of unsaturated air with cloudy air and cloud top. Solar absorption later in the observing period may stabilize the cloud layer and counteract the destabilization due to longwave radiative cooling and contribute to the observed reduction of the turbulence intensity later in the observing period. The skewness profiles obtained early in the observing period are positive in the upper part of the layer and negative lower in the layer. These profiles are consistent with relatively narrow updrafts at cloud top and narrow downdrafts lower in the cloud.

Spectra analyses at different levels in the cloud reveal the different scales of motion associated with the turbulence. In-cloud vertical velocity spectra show variability at scales smaller than the 1-km peak in the spectrum of the cloud-top height. Spectral peaks on scales of 100–400 m are consistent with relatively strong updrafts and downdrafts observed in the cloud.

A conditional sampling technique was applied to the data to further examine the structure of coherent eddies in the cloud. Eighty percent of radar grid points that experience a perturbation upward velocity were found to be associated with vertical coherent structures rather than isolated upward-moving cloud elements. Fractional coverage of updrafts and mass fluxes from the conditional sampling were compared with the estimates of these quantities made using the R92 method. These comparisons are remarkably similar to those made by R92 using the LES vertical velocity fields. Additional definition of the turbulence structure of the cloud was obtained by sampling updrafts and downdrafts with selection criteria over a range of cutoff velocities.

The structure of the coherent updrafts and eddies and their relationship to the entrainment zone was studied by examining vertical velocities and reflectivity gradients at cloud top. Although broad areas ($\approx$1 km) of updraft that correspond to the variability in the cloud-top height are identified, there is considerable variability within these regions. Well-defined updraft cores with horizontal scales of 100–400 m dominate this variability. The entrainment zone was relatively thick in areas where downdrafts were observed near cloud top and thin in the regions of updrafts. These results provide evidence that entrainment in this case is occurring on scales that are consistent with engulfment at cloud top (large-scale mixing), although we cannot rule out the possibility that air experiencing interfacial small-scale mixing at the cloud peaks may be feeding these engulfments zones.

The relative uniform cloud boundaries and the nighttime and early morning character of the observations provide a unique case study of a buoyancy driven cloud-topped boundary layer. In addition, these data provide new insight into large-eddy structures that extend through the depth of the cloud. The high vertical resolution, time-evolving turbulence statistics that were obtained in this study would be impossible to obtain directly from aircraft observations. Furthermore, the radar observations provide a description of the vertical structure of the large eddies that cannot be defined from aircraft except by compositing structures obtained on consecutive flight legs at different levels (e.g., Wang and Albrecht 1994). Unfortunately, millimeter-wavelength radars do not provide a complete description of the cloud structure. Although microphysical retrievals for these radars continue to be developed (e.g., Sassen and Liao 1996; Babb et al. 1999), the routine applications of these techniques to obtain the microphysical structure at high temporal resolution has not been demonstrated. Although combinations of remote sensing systems can aid in the definition of the in-cloud microphysical structure, it is difficult to measure the thermodynamic variability at resolutions that are consistent with the radar sampling. Furthermore, the presence of drizzle can complicate the retrieval of vertical air motions in boundary layer clouds. Although drizzle did not appear to be a limiting factor in our study, many stratocumulus clouds may have much higher drizzle rates (Fox and Illingworth 1997). Babb and Verlinde (1999) demonstrate how Doppler spectra from a millimeter-wavelength radar can be used to obtain vertical velocity statistics in a cloud with drizzle. As the retrieval techniques for cloud radar become more sophisticated it will be possible to further advance our understanding by providing critical large eddy observations (LEO) for process studies and the direct evaluation of LES models.

Acknowledgments. We acknowledge all those responsible for the planning and execution of the Continental Stratus Experiment and we are particularly appreciative of the efforts of David Babb, Gerald Mace, Robert Peters, and William Syrett. In addition, we thank Eugene E. Clothiaux for his expert advice and assistance with the processing of the data. This re-

Unauthenticated | Downloaded 04/21/24 11:41 PM UTC

search was funded by NSF Grant ATM9730119 and DOE Grant DEFG0297ER62337.

REFERENCES

Albrecht, B. A., R. Penc, and W. H. Schubert, 1985: An observational study of cloud-topped mixed layer. *J. Atmos. Sci.*, **42,** 800–822.

——, C. W. Fairall, D. W. Thomson, A. B. White, J. B. Snider, and W. H. Schubert, 1990: Surface-based remote sensing of the observed and the adiabatic liquid water content of stratocumulus clouds. *Geophys. Res. Lett.*, **17,** 89–92.

Babb, D., and J. Verlinde, 1999: Vertical velocity statistics in continental stratocumulus clouds as measured by a 94 GHz radar. *Geophy. Res. Lett.*, **26,** 1177–1180.

——, ——, and B. A. Albrecht, 1999: Retrieval of cloud microphysical parameters from 94 GHz radar Doppler power spectra. *J. Atmos. Oceanic Technol.*, **16,** 489–503.

Brost, R. A., D. H. Lenschow, and J. C. Wyngaard, 1982: Marine stratocumulus layers. Part II: Turbulence budgets. *J. Atmos. Sci.*, **39,** 818–836.

Caughey, S. J., B. A. Crease, and W. T. Roach, 1982: A field study of nocturnal stratocumulus. II: Turbulence structure and entrainment. *Quart. J. Roy. Meteor. Soc.*, **108,** 125–144.

Clothiaux, E. E., M. A. Miller, B. A. Albrecht, T. P. Ackerman, J. Verlinde, D. M. Babb, R. M. Peter, and W. J. Syrett, 1995: An evaluation of a 94-GHz radar for remote sensing of cloud properties. *J. Atmos. Oceanic Technol.*, **12,** 201–229.

Del Genio, A. D., M.-S. Yao, W. Kovari, and K. K.-W. Lo, 1996: A prognostic cloud water parameterization for global climate models. *J. Climate*, **9,** 270–304.

Fox, N. I. and A. J. Illingworth, 1997: The retrieval of stratocumulus cloud properties by groud-based cloud radar. *J. Appl. Meteor.*, **36,** 465–492.

Frisch, A. S., C. W. Fairall, and J. B. Snider, 1995a: Measurement of stratus cloud and drizzle parameters in ASTEX with a K_α-band doppler radar and microwave radiometer. *J. Atmos. Sci.*, **52,** 2788–2799.

——, D. H. Lenschow, C. W. Fairall, W. H. Schubert, and J. S. Gibson, 1995b: Doppler radar measurements of turbulence in marine stratiform cloud during ASTEX. *J. Atmos. Sci.*, **52,** 2800–2808.

Gray, G. R., C. A. Walther, R. J. Keeler, C. L. Frush, and J. R. Vinson, 1989: A new programmable signal processor for NCAR meteorological radars. Preprints, *24th Conf. on Radar Meteorology*, Tallahassee, FL, Amer. Meteor. Soc., 447–450.

Han, Y., and D. W. Thomson, 1994: Multichannel microwave radiometric observations at Saipan during the 1990 Tropical Cyclone Motion Experiment. *J. Atmos. Oceanic Technol.*, **11,** 110–121.

Hignett, P., 1991: Observations of diurnal variation in a cloud-capped marine boundary layer. *J. Atmos. Sci.*, **48,** 1474–1482.

Jensen, N. O., and D. H. Lenschow, 1978: An observational investigation of penetrative convection. *J. Atmos. Sci.*, **35,** 1924–1933.

Karl, T. R., and Coauthors, 1993: A new perspective on recent global warming: Asymmetric trends of daily maximum and minimum temperature. *Bull. Amer. Meteor. Soc.*, **74,** 1007–1023.

Kitchen, M., and S. J. Caughey, 1981: Tethered-balloon observations of the structure of small cumulus clouds. *Quart. J. Roy. Meteor. Soc.*, **107,** 853–874.

Le Mone, M. A., 1990: Some observations of vertical velocity skewness in the convective planetary boundary layer. *J. Atmos. Sci.*, **47,** 1163–1169.

Lenschow, D. H., and P. L. Stephens, 1980: The role of thermals in the convective boundary layer. *Bound.-Layer Meteor.*, **19,** 509–532.

Lhermitte, R. M., 1987: A 94-GHz Doppler radar for cloud observations. *J. Atmos. Oceanic Technol.*, **4,** 36–48.

Miller, M. A., and B. A. Albrecht, 1995: Surface-based observations of mesoscale cumulus–stratocumulus interaction during ASTEX. *J. Atmos. Sci.*, **52,** 2809–2826.

Moeng, C.-H., 1986: Large-eddy simulation of a stratus-topped boundary layer. Part I: Structure and budgets. *J. Atmos. Sci.*, **43,** 2886–2900.

——, and R. Rotunno, 1990: Vertical-velocity skewness in the buoyancy-driven boundary layer. *J. Atmos. Sci.*, **47,** 1149–1162.

——, S. Shen, and D. A. Randall, 1992: Physical processes within the nocturnal stratocumulus cloud layer. *J. Atmos. Sci.*, **49,** 2384–2401.

——, and Coauthors, 1996: Simulation of a stratocumulus-topped PBL: Intercomparison among different numerical codes. *Bull. Amer. Meteor. Soc.*, **77,** 261–278.

Moyer, K. A., and G. S. Young, 1991: Observations of vertical velocity skewness within the marine stratocumulus-topped boundary layer. *J. Atmos. Sci.*, **48,** 403–410.

Nicholls, S., 1989: The structure of radiatively-driven convection in stratocumulus. *Quart. J. Roy. Meteor. Soc.*, **115,** 487–511.

Penc, R. S., and B. A. Albrecht, 1987: Parametric representation of heat and moisture fluxes in cloud-topped layers. *Bound.-Layer Meteor.*, **38,** 225–248.

Peters, R. M., B. A. Albrecht, and M. A. Miller, 1993: Marine boundary layer cloud profiling with a 94 GHz radar. Preprints, *Eighth Symp. on Meteorology Observations and Instrumentation*, Anaheim, CA, Amer. Meteor. Soc., 205–208.

Ramanathan, V., R. D. Cess, E. F. Harrison, P. Minnis, B. R. Barkstrom, E. Ahmad, and D. Hartmann, 1989: Cloud-radiative forcing and climate: Results from the Earth Radiation Budget Experiment. *Science*, **243,** 57–63.

Randall, D. A., Q. Shao, and C.-H. Moeng, 1992: A second-order bulk boundary-layer model. *J. Atmos. Sci.*, **49,** 1903–1923.

Sassen, K., and L. Liao, 1996: Estimation of cloud content by W-band radar. *J. Appl. Meteor.*, **35,** 932–938.

——, G. G. Mace, Z. Wang, M. R. Poellot, S. M. Sekelsky, and R. E. McIntosh, 1999: Continental stratus clouds: A case study using coordinated remote sensing and aircraft measurements. *J. Atmos. Sci.*, **56,** 2345–2358.

Vali, G., R. Kelly, J. French, S. Haimov, D. Leo, R. McIntosh, and A. Pazmany, 1998: Fine-scale structure and microphysics of coastal stratus. *J. Atmos. Sci.*, **55,** 3540–3564.

Wang, Q., and B. A. Albrecht, 1994: Observations of cloud-topped entrainment in marine stratocumulus. *J. Atmos. Sci.*, **51,** 1530–1547.

Wang, S., and B. A. Albrecht, 1986: A stratocumulus model with an internal circulation. *J. Atmos. Sci.*, **43,** 2373–2391.

——, and B. Stevens, 2000: Top-hat representation of turbulence statistics in cloud-topped boundary layers: A large eddy simulation study. *J. Atmos. Sci.*, **57,** 423–441.

Warner, J., 1977: Time variation of updraft and water content in small cumulus clouds. *J. Atmos. Sci.*, **34,** 1306–1312.

Wyant, M. C., C. S. Bretherton, H. A. Rand, and D. E. Stevens, 1997: Numerical simulations and a conceptual model of the stratocumulus to trade cumulus transition. *J. Atmos. Sci*, **54,** 168–192.

Zhou, M.-Y., D. H. Lenschow, B. B. Stankov, J. C. Kaimal, and J. E. Gaynor, 1985: Wave and turbulence structure in a shallow baroclinic convective boundary layer and overlying inversion. *J. Atmos. Sci.*, **42,** 47–57.

Unauthenticated | Downloaded 04/21/24 11:41 PM UTC